Energy & Environmental Science

ROYAL SOCIETY OF CHEMISTRY

PAPER

View Article Online
View Journal | View Issue

Cite this: *Energy Environ. Sci.*, 2024, **17**, 5191

An efficient alkoxy-substituted polymer acceptor for efficient all-polymer solar cells with low voltage loss and versatile photovoltaic applications†

Han Yu, ‡*[ab] Chaoyue Zhao, ‡[bc] Huawei Hu, *[ad] Shenbo Zhu,[a] Bosen Zou,[b] Top Archie Dela Peña,[ef] Ho Ming Ng,[b] Chung Hang Kwok,[b] Jicheng Yi,[b] Wei Liu,[b] Mingjie Li,[f] Jiaying Wu,[e] Guangye Zhang,*[c] Yiwang Chen[ad] and He Yan*[b]

All-polymer solar cells (all-PSCs) have emerged as promising candidates for practical applications owing to their excellent stability and mechanical durability. Despite these merits, the device performance of all-PSCs still falls behind those based on small-molecule acceptors. The critical challenge lies in balancing and enhancing both the open-circuit voltage (V_{OC}) and the short-circuit current density (J_{SC}) in a synergistic manner. Herein, we designed an acceptor, PYO-V, with upshifted energy levels as well as blue-shifted absorption by linking alkoxy side chains on the β position of the outer thiophene units. The introduction of PYO-V into the PM6:PY-V-γ host system complements its absorption spectrum, improving its molecular packing, suppressing its charge recombination, and enhancing its polaron generation efficiency. Consequently, the resulting ternary all-PSCs with 20 wt% PYO-V achieved a significantly enhanced efficiency of 18.5%, which represents the highest value for reported all-PSCs with a V_{OC} of over 0.93 V. Moreover, the hypsochromic PYO-V also displays its versatile applications in indoor photovoltaics, as the PYO-V-based binary device achieves an efficiency of over 24%, among the best performance for indoor all-PSCs. This work presents an effective strategy for designing polymer acceptors with wider bandgaps for outdoor and indoor photovoltaic applications.

Received 24th April 2024,
Accepted 28th May 2024

DOI: 10.1039/d4ee01804d

rsc.li/ees

Broader context

Organic solar cells (OSCs) have emerged as a promising solar technology due to their lightweight nature, flexibility, and facile roll-to-roll fabrication processes. However, commercialization of OSCs has been limited by their relatively low stability. To this end, researchers have concentrated on the development of all-polymer solar cells (all-PSCs), which have shown excellent stability and robust mechanical toughness for commercial applications. This research article presents a novel approach to improve the efficiency of all-PSCs by introducing alkoxy-substituted polymer acceptors. The results demonstrate that this approach can effectively fine-tune the optoelectrical properties of polymer acceptors, leading to efficient all-PSCs for versatile photovoltaic applications. The introduction of alkoxy-substituted polymer acceptors complements the absorption spectrum and effectively suppresses energy losses in all-PSCs, resulting in significantly improved efficiency and stability. The development of efficient and stable OSCs is crucial for the widespread adoption of solar energy as a clean and renewable energy source. This study contributes to the growing body of literature on the development of OSCs and provides a promising avenue for the commercialization of all-PSCs. With the demand for energy sources, the development of efficient and stable OSCs has the potential to revolutionize the energy industry and contribute to a sustainable future.

[a] *State Key Laboratory for Modification of Chemical Fibers and Polymer Materials, College of Materials Science and Engineering, Donghua University, Shanghai 201620, China. E-mail: huaweihu@dhu.edu.cn*

[b] *Department of Chemistry, Guangdong-Hong Kong-Macao Joint Laboratory of Optoelectronic and Magnetic Functional Materials, Energy Institute and Hong Kong Branch of Chinese National Engineering Research Center for Tissue Restoration & Reconstruction, Hong Kong University of Science and Technology, Clear Water Bay, Kowloon, Hong Kong 999077, China. E-mail: hyuak@connect.ust.hk, hyan@ust.hk*

[c] *College of New Materials and New Energies, Shenzhen Technology University, Shenzhen 518118, China. E-mail: zhangguangye@sztu.edu.cn*

[d] *Key Lab of Fluorine and Silicon for Energy Materials and Chemistry of Ministry of Education/National Engineering Research Center for Carbohydrate Synthesis, Jiangxi Normal University, 99 Ziyang Avenue, Nanchang 330022, China*

[e] *Advanced Materials Thrust, Function Hub, The Hong Kong University of Science and Technology, Nansha, Guangzhou 511400, China*

[f] *The Hong Kong Polytechnic University, Faculty of Science, Department of Applied Physics, Kowloon, Hong Kong 999077, China*

† Electronic supplementary information (ESI) available. See DOI: https://doi.org/10.1039/d4ee01804d

‡ H. Yu, and C. Z. contributed equally to this work.

Introduction

Organic solar cells (OSCs) have demonstrated their great potential as one of the most promising emerging solar technologies due to their advantages of lightweightness, flexibility and compatibility with the roll-to-toll fabrication process.[1–4] Through numerous research efforts devoted to material development and device optimization,[5–8] the power conversion efficiencies (PCEs) of small-molecular acceptor (SMA)-based OSCs have exceeded 19%,[9–12] attracting considerable attention from both the academia and the industry. However, device stability is still a critical aspect that limits the commercialization of SMA-based OSCs. To overcome this issue, all-polymer solar cells (all-PSCs), which adopt polymers as both donors and acceptors (Fig. S1, ESI†), have become a recent hot topic in the OSC community due to their extra advantages of excellent light/thermal stability and robust mechanical toughness for commercial application.[13–15] Benefitting from the development of Y-series SMAs[16–19] and their derived polymerized-SMAs (Fig. S2, ESI†),[20–24] the PCEs of all-PSCs based on Y-series polymer acceptors have surpassed 17%.[25–29]

Despite these advantages, the device performance of all-PSCs still trails behind those of their counterparts based on SMAs. The primary challenge lies in synergistically balancing the trade-off between the open-circuit voltage (V_{OC}) and the short-circuit current density (J_{SC}). To further improve the efficiencies of all-PSCs, the ternary tactic has been an effective and facile approach that introduces a third component into binary systems.[30,31] As for the third component, one of the effective guest materials for ternary all-PSCs is polymer acceptors with structures similar to that of the host, which could fine-tune the morphology and molecular crystallinity.[32] However, the majority of Y-series polymer acceptors reported to date exhibit overlapping absorption spectra and energy levels, which contradict the principle of utilizing materials with complementary absorption and effective energy loss management in ternary devices to maximize the device performance. Replacing the alkyl side chains with alkoxy side chains at the β position of the outer thiophene in Y-series SMAs has been demonstrated as an effective approach to blue shift the absorption of SMAs with a higher occupied LUMO level, due to the weaker intramolecular charge transfer (ICT) effect by alkoxylation.[33] Moreover, the alkoxy acceptors are beneficial for achieving panchromatic absorption and suppressing voltage loss in ternary devices.[34,35] Besides the outdoor OSCs, the absorption of the alkoxy acceptors is matchable with the LED light source, which is also applicable to indoor photovoltaics.[36] Therefore, it is anticipated to adjust the absorption spectra and the energy level of Y-series polymer acceptors in order to achieve efficient and stable all-PSCs for both outdoor and indoor applications.

In this work, we investigated the alkoxy substitution for the construction of Y-series polymer acceptors for all-PSC operations. One alkoxy-substituted polymer acceptor (PYO-V) with a conventional Y-series central core on the thiophene moiety was synthesized and systematically studied (Fig. 1). It is found that alkoxy-substituted PYO-V exhibits hypsochromic absorption and an up-shifted LUMO level relative to the classical PY-V-γ, due to the weaker ICT effect. The introduction of PYO-V into the PM6:PY-V-γ host system complements its absorption spectrum and effectively manages the energy loss. As a result, the PM6:PY-V-γ:PYO-V ternary all-PSCs achieved an outstanding efficiency of 18.5%, much higher than that of PM6:PY-V-γ-based devices (17.3%), with a V_{OC} of 0.932 V and a J_{SC} of 25.9 mA cm^{-2}. Further investigation of the blend morphology revealed that the ternary blend shows a stronger crystallinity and favorable phase segregation when mixed with 20 wt%

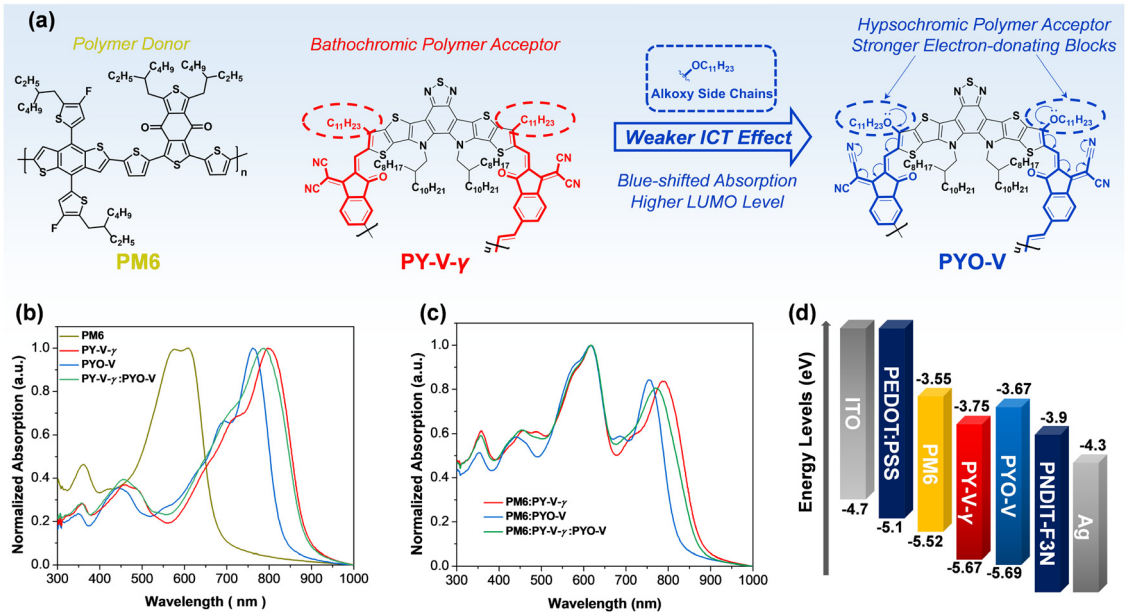

Fig. 1 (a) Chemical structures of PM6 (polymer donor), PY-V-γ (bathochromic polymer acceptor), and PYO-V (hypsochromic polymer acceptor). Normalized UV-Vis absorption spectra of (b) PM6, PY-V-γ, PYO-V, and PY-V-γ:PYO-V films and (c) PM6:PY-V-γ, PM6:PYO-V, and PM6: PY-V-γ:PYO-V blend films. (d) Energy alignment of materials in all-PSCs.

PYO-V, thus leading to efficient charge transport and a lower extent of charge recombination. Besides outdoor photovoltaics, PYO-V also presents its versatile applications in indoor photovoltaics, achieving an efficiency of 24.0% in binary devices, which is among the highest efficiencies for indoor all-PSCs. Our work demonstrates that alkoxy substitution is an effective strategy for tuning the optoelectrical properties of polymer acceptors and achieving efficient all-PSCs for versatile photovoltaic applications.

Results and discussion

The chemical structures of PM6, PY-V-γ, and PYO-V are shown in Fig. 1a. The synthesis details of PYO-V with vinylene as the linkage for a rigid and co-planar conformation are summarized in the ESI.† [27] Density functional theory (DFT) calculations were performed at the B3LYP/6-31G* level to study the effects of alkoxy groups on the molecular geometry and optoelectrical properties (Fig. S3, ESI†).[37] Compared to PY-V-γ, the electron distribution of PYO-V's frontier molecular orbitals extended to the alkoxy side chain, implying a wider conjugation between alkoxy chains and the central backbone. The alkoxy groups could donate electrons to reduce the electron deficiency of the end group moiety, resulting in PYO-V with a larger bandgap and a higher occupied LUMO level relative to those of PY-V-γ. Fig. 1b exhibits the normalized ultraviolet-visible (UV-vis) absorption spectra of PM6, PY-V-γ, PYO-V, and PY-V-γ:PYO-V in thin films. Compared to PY-V-γ which owns a maximum absorption peak ($\lambda_{max,film}$) located at 746 nm, the alkoxy-substituted PYO-V exhibits a hypsochromic shift in the absorption peak. The optical bandgaps (E_g) of PY-V-γ and PYO-V are found to be 1.31 and 1.47 eV, respectively, calculated from their corresponding absorption onsets. The blue-shifted $\lambda_{max,film}$ of PYO-V is due to the weaker ICT effect caused by the alkoxy groups. Consequently, PYO-V exhibits complementary absorption characteristics when combined with PM6:PY-V-γ. Upon the addition of 20 wt% PYO-V, the ternary systems demonstrate enhanced absorption compared to that of the binary blends (Fig. 1c), facilitating improved photon harvesting and photocurrent generation. Additionally, cyclic voltammetry (CV, Fig. 1d and Fig. S4, ESI†) measurements reveal that PYO-V has a higher LUMO level compared to PY-V-γ. Both the absorption and CV results align with the trends predicted by DFT calculations.

The photovoltaic performance of these all-polymer active layer combinations under AM 1.5G (100 mW cm^{-2}) illumination was investigated through a conventional device structure of indium tin oxide (ITO)/poly(3,4-ethylenedioxythiophene):polystyrene sulfonate (PEDOT:PSS)/PM6:polymer acceptors/PNDIT-F3N/Ag. PM6 was used for its complementary absorption and suitable energy level alignment with the polymer acceptors mentioned in this work and was purchased from Volt-Amp Optoelectronics Tech. Co., Ltd, Dongguan, China. The device properties of all-PSCs under optimal processing conditions are summarized in Table 1 and the J–V curves are plotted in Fig. 2a. The PM6:PY-V-γ-based device yields a PCE of 17.3%, with a V_{OC} of 0.909 V, a J_{SC} of 25.2 mA cm^{-2} and an FF of 75.7%. In contrast, the PYO-V-based device shows a higher V_{OC} (0.975 V) than that of the PY-V-γ-based one because of a relatively higher LUMO level, while the J_{SC} (19.6 mA cm^{-2}) and FF (69.4) of the device based on PM6:PYO-V are obviously lower than those of the reference PY-V-γ-based device, leading to a lower PCE of 13.3%. Interestingly, when we introduced PYO-V as the guest component into the PM6:PY-V-γ system to fabricate ternary devices, the performance improved effectively with a PCE of 18.5%, which is mainly ascribed to higher and more balanced carrier mobilities and higher EQE values in the range of 650–850 nm. Fig. 2b displays the external quantum efficiency (EQE) curves of these two devices to explain the difference in the J_{SC} values between these devices. The calculated J_{SC} values of PM6:PY-V-γ, PM6:PYO-V and ternary-based devices are 24.1, 19.0 and 24.9 mA cm^{-2}, respectively, well consistent with the tested J_{SC} measured from the J–V curves within ±5% error (Table 1).

To investigate the charge recombination kinetics within the devices, we initially evaluated the dependence of V_{OC} on P_{light}[38] and subsequently calculated the ideality factor ($n_{id,l}$) using the equation $n_{id,l} = \frac{q}{kT}\frac{\partial V_{oc}}{\partial \ln(I)}$. Here, a $n_{id,l}$ value approaching 1 indicates bi-molecular recombination dominance, while a value close to 2 indicates trap-assisted recombination dominance. As depicted in Fig. S5 (ESI†), the PM6:PYO-V blend exhibits the highest $n_{id,l}$ value of 1.50, followed by PM6:PY-V-γ with 1.34 and the ternary device displaying the lowest $n_{id,l}$ value of 1.22. Subsequently, to reaffirm the validity of the $n_{id,l}$ values, we performed the dark J–V test and obtained the $n_{id,d}$ values using the formula $n_{id,d} = \frac{q}{kT}\frac{\partial V}{\partial J}$ (Fig. 2c), which exhibits a similar trend to $n_{id,l}$. In addition, the dependence of J_{SC} on P_{light} (Fig. S5, ESI†) indicates that the three devices have similar bimolecular recombination. These results indicate that incorporating PYO-V into the PM6:PY-V-γ system can reduce the trap-assisted recombination pathway of the ternary blends. Furthermore, the charge-transporting behaviors of the three systems were studied using the space-charge-limited current (SCLC) method (Fig. S6, ESI†).[39] The hole mobility (μ_h) and electron mobility (μ_e) of the PM6:PY-V-γ based system are 3.62 × 10^{-4} cm^2 V^{-1} s^{-1} and 3.84 × 10^{-4} cm^2 V^{-1} s^{-1}, respectively (Table 1). The introduction of

Table 1 Summary of device parameters of the optimized OSCs

Active layer	V_{OC} (V)	J_{SC} (mA cm^{-2})	J_{EQE} (mA cm^{-2})	FF (%)	PCE[a] (%)	μ_h (cm^2 V^{-1} s^{-1})	μ_e (cm^2 V^{-1} s^{-1})
PM6:PY-V-γ	0.909 ± 0.004 (0.909)	24.7 ± 0.5 (25.2)	24.1	75.3 ± 0.8 (75.7)	17.0 ± 0.3 (17.3)	3.62 × 10^{-4}	3.84 × 10^{-4}
PM6:PYO-V	0.970 ± 0.005 (0.975)	19.1 ± 0.5 (19.6)	19.0	68.9 ± 1.8 (69.4)	12.8 ± 0.5 (13.3)	3.37 × 10^{-4}	3.10 × 10^{-4}
PM6:PY-V-γ:PYO-V	0.931 ± 0.004 (0.932)	25.9 ± 0.2 (25.9)	24.9	75.7 ± 0.4 (76.5)	18.2 ± 0.3 (18.5)	3.75 × 10^{-4}	3.82 × 10^{-4}

[a] The standard deviations are based on measurements of over at least 20 independent devices.

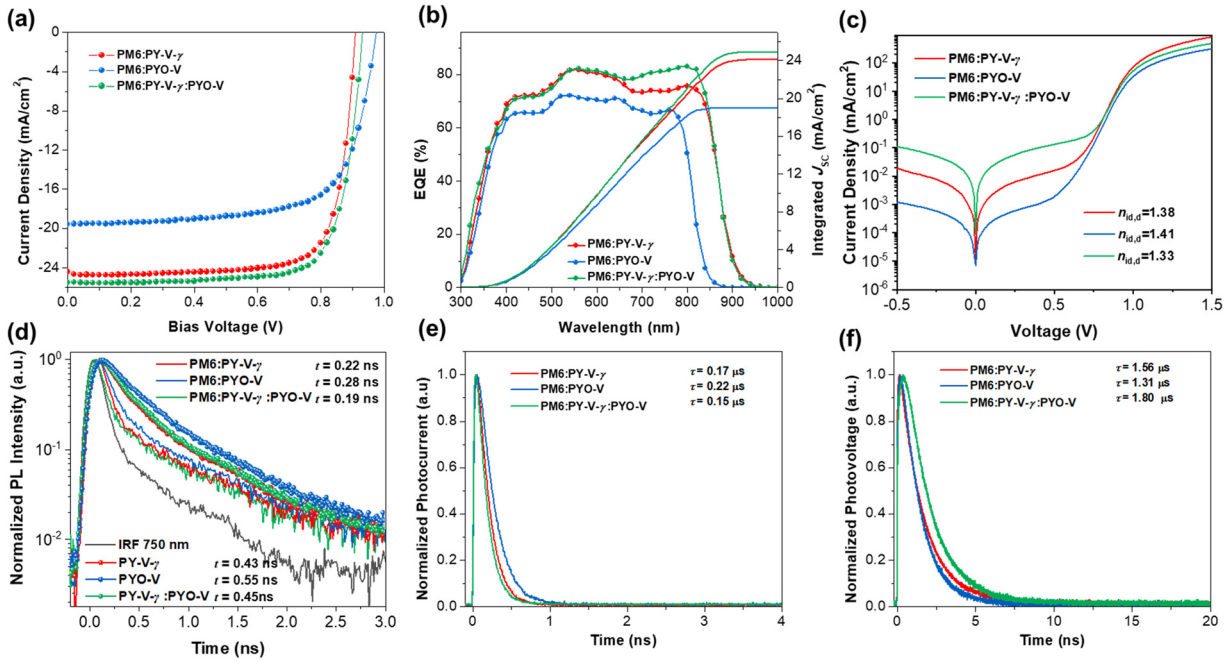

Fig. 2 (a) *J*–*V* characteristics and (b) external quantum efficiency (EQE) spectra and (c) dark *J*–*V* curves of the three types of all-PSCs. (d) TR-PL decay curves of the PY-V-γ, PYO-V, and PY-V-γ:PYO-V neat films and the PM6:PY-V-γ, PM6:PYO-V and PY-V-γ:PYO-V blend films. The pump and probe wavelengths are 750 nm. (e) TPC and (f) TPV spectra of the four all-polymer devices.

PYO-V into the PM6:PY-V-γ system led to a more balanced charge transport, evidenced by the μ_h/μ_e value of 1.01, compared to 1.06 in the host system. The more balanced charge carrier mobilities of the ternary system are consistent with the excellent photovoltaic performance.

Time-resolved photoluminescence (TR-PL) characterization studies were performed to study their exciton dissociation behaviors (Fig. 2d). Pure PY-V-γ exhibited a PL decay lifetime of 0.43 ns, which decreased to 0.22 ns after mixing with PM6. Upon the addition of the acceptor PYO-V as the third component, the PL quenching process accelerated further to 0.19 ns, suggesting that the addition of PYO-V promotes exciton dissociation. To further examine carrier recombination and carrier extraction, the transient photovoltage (TPV) and transient photocurrent (TPC) tests were performed.[40] As shown in Fig. 2e, TPC measurements show that the photocurrent decay lifetimes of PM6:PY-V-γ, PM6:PYO-V, and PM6:PY-V-γ:PYO-V are 0.17, 0.22, and 0.15 μs, respectively. Additionally, the photovoltage decay times of PM6:PY-V-γ, PM6:PYO-V, and PM6:PY-V-γ:PYO-V are 1.56, 1.31, and 1.80 μs, respectively (Fig. 2f). The shorter charge extraction time and the longer carrier lifetime demonstrate that the ternary all-PSC has the lowest charge recombination rate.

The vertical phase distribution within the active layer plays a crucial role in determining the device performance. To directly probe this distribution, we performed film-depth-dependent light absorption spectroscopy (FLAS).[37,41] Fig. S7 (ESI†) shows the FLAS results and the ratio of the acceptor PY-V-γ relative to the donor PM6 for binary and ternary films. The results indicate that the ratio of the PY-V-γ acceptor is higher near both the electron transport layer (ETL) and hole transport layer (HTL) interfaces compared to that of the donor PM6, potentially leading to increased carrier recombination in the PM6:PY-V-γ-based device. However, upon the addition of 20% PYO-V, this distribution changed, with the ratios of donor and acceptors becoming nearly equal near the HTL interface, resulting in a more efficient hole transport within the ternary system. Moreover, the exciton generation rate map (Fig. S8, ESI†) shows that the ternary all-PSCs exhibit the highest exciton generation rate in the middle part of the active layer. These results support the enhanced device performance achieved for the ternary devices.

Continuing from the vertical phase distribution, atomic force microscopy (AFM) was utilized to investigate the surface morphology of the blend films. The height images (Fig. S9, ESI†) show that all three blend films have relatively smooth surfaces with root-mean-square roughness (R_q) values of 1.11, 1.36, and 1.12 nm for PM6:PY-V-γ, PM6:PYO-V, and PM6: PY-V-γ:PYO-V, respectively. Furthermore, grazing incidence wide-angle X-ray scattering (GIWAXS) measurements were used to correlate the free charge properties with the morphological features of pure and blend polymer acceptor films. As shown in Fig. S10 (ESI†), the introduction of PYO-V into pristine PY-V-γ films results in blend acceptor films with a stronger intensity compared to that of pure PY-V-γ films, suggesting that PYO-V could aid in the molecular packing of PY-V-γ. After blending with the donor, both binary and ternary D/A films exhibited face-on orientation with the (010) stacking peaks located at $q_z \approx 1.73$ Å^{-1} (Fig. 3a and b). Additionally, the ternary-based blend films exhibited slightly larger (010) crystallite coherence length (CCL) values compared to those of the other two binary blend films (Table S1, ESI†). This enhancement in CCL facilitates charge transport and suppresses charge recombination within the ternary blend films, contributing to improved device

performance. To further investigate the phase-separation behavior of the blend films, resonant soft X-ray scattering (RSoXS) measurements were carried out.[42] Fig. 3c displays the Lorentz-corrected RSoXS profiles of the different blend films, where both blends exhibit two log-normal peaks. The relative domain purity for PM6:PY-V-γ, PM6:PYO-V, and PM6:PY-V-γ:PYO-V is 0.90, 1, and 0.94, respectively. Although PM6:PYO-V exhibited the highest domain purity, it only exhibited a relatively large length-scale phase separation with a long period of 83 nm. In contrast, PY-V-γ-based binary and ternary films exhibit two log-normal peaks. The low-q and high-q peaks are located around 0.048/0.195 and 0.049/0.186 nm^{-1}, respectively, corresponding to the domain spacing of ~131/32 and ~128/34 nm for PM6:PY-V-γ and PM6:PY-V-γ:PYO-V-based blend films (Table S2, ESI†), respectively. This observation highlights that the inclusion of 20% PYO-V can preserve the multi-length scale morphology while enhancing the domain purity of PM6:PY-V-γ, leading to the suppression of bimolecular recombination and enhanced charge collection in the ternary devices.[43]

Exciton dynamics of the pristine (Fig. S11, ESI†) and blend films (Fig. 4a–c) were investigated by transient absorption spectroscopy (TAS).[44] Fig. 4d illustrates the singlet exciton decay dynamics of the acceptor neat films based on their photo-induced absorption (PIA). PYO-V has a significantly slower exciton decay at 15.79 ns, while PY-V-γ and PY-V-γ:PYO-V have virtually identical decay times (7.85 ns and 7.58 ns, respectively). This implies that the exciton contribution from the acceptor in the ternary blend is dominated by PY-V-γ. Fig. 4e shows the dynamics of polaron generation (580–590 nm probe) for the binary and ternary blends based on the evolution of polaron photo bleach (PB). Despite the significantly slower polaron generation from PM6:PYO-V (10.13 ps), the PM6:PY-V-γ-PYO-V ternary blend (3.77 ps) outperformed PM6:PY-V-γ (5.76 ps). It can be deduced that the faster polaron generation contributes to the superior J_{SC} of the ternary blend. Considering the exciton decay dynamics in Fig. 4d, this enhancement should be attributed to optimized donor–acceptor interface morphology after the incorporation of PYO-V. From Fig. 4f, it can be seen that the sub-ns free charge recombination based on polaron PB decay has not been affected by the incorporation of PYO-V. Therefore, the drop in FF for the ternary blend is unlikely to be ascribed to bimolecular recombination, which resonates with the light intensity-dependent experiments.

Addressing the challenge of improving the PCE while simultaneously minimizing the energy loss (E_{loss}) is crucial,[45] particularly in the context of all-PSCs. The overall E_{loss} can be decomposed into three components, ΔE_1, ΔE_2, and ΔE_3, where ΔE_1 ($E_g - V_{OC,sq}$) denotes radiative recombination loss occurring above the bandgap, ΔE_2 ($V_{OC,sq} - V_{OC,rad}$) signifies radiative recombination loss below the bandgap, and ΔE_3 accounts for non-radiative recombination loss.[46] To comprehensively elucidate the rise in V_{OC} in OSC devices employing the PYO-V acceptor, Fourier-transform photocurrent spectroscopy (FTPS)-EQE (Fig. 5a–c) and electroluminescence quantum yield (EQE_{EL}, Fig. 5d) experiments were conducted to quantify the energy loss, and detailed parameters are listed in Table S3 (ESI†). As shown in Fig. 5e, the PM6:PYO-V-based device exhibits a slightly larger ΔE_1 which should be attributed to its larger energy gaps. The ΔE_2 values are calculated to be 0.050, 0.083, and 0.049 eV for PM6:PY-V-γ, PM6:PYO-V, and PM6:PY-V-γ:PYO-V, respectively, owing to a larger HOMO level offset between PM6 and PYO-V. Significantly, notable distinctions were identified in the ΔE_3 values among the blends. Specifically, the ΔE_3 value of the PM6:PY-V-γ:PYO-V-based OSC (0.188 eV) is substantially lower than that of the PM6:PY-V-γ (0.202 eV) and the PM6:PYO-V-based device (0.220 eV), indicating that the incorporation of PYO-V into the PM6:PY-V-γ blend effectively diminishes the nonradiative recombination loss. Consequently, PM6:PY-V-γ:PYO-V exhibited a minimum voltage loss of 0.499 eV, which is much lower than those of PM6:PY-V-γ (0.514 eV) and PM6:PYO-V (0.574 eV). To the best of our knowledge, the E_{loss} of

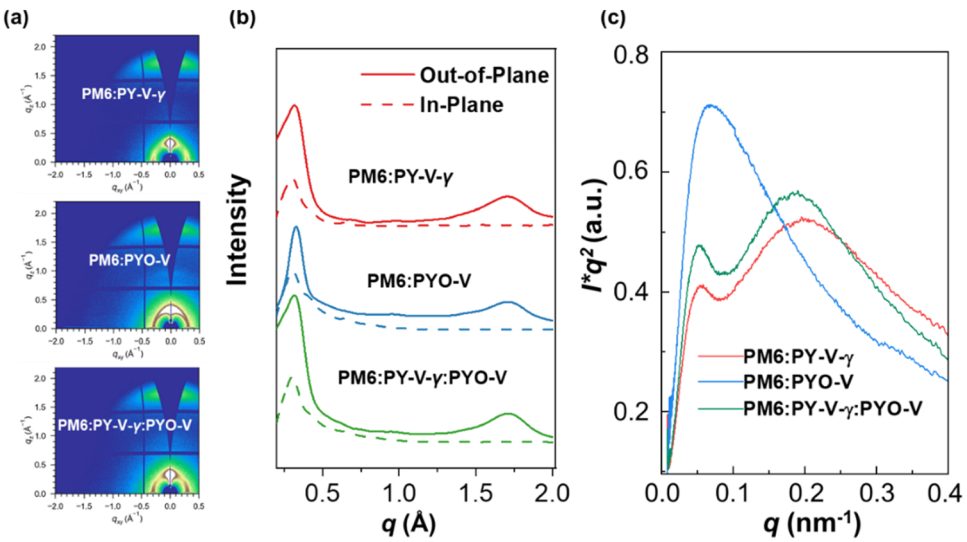

Fig. 3 (a) 2D-GIWAXS patterns of blend films. (b) Line cuts of the 2D GIWAXS patterns for the blend films. (c) Lorentz-corrected RSoXS scattering profiles of blend films acquired at 284.8 eV.

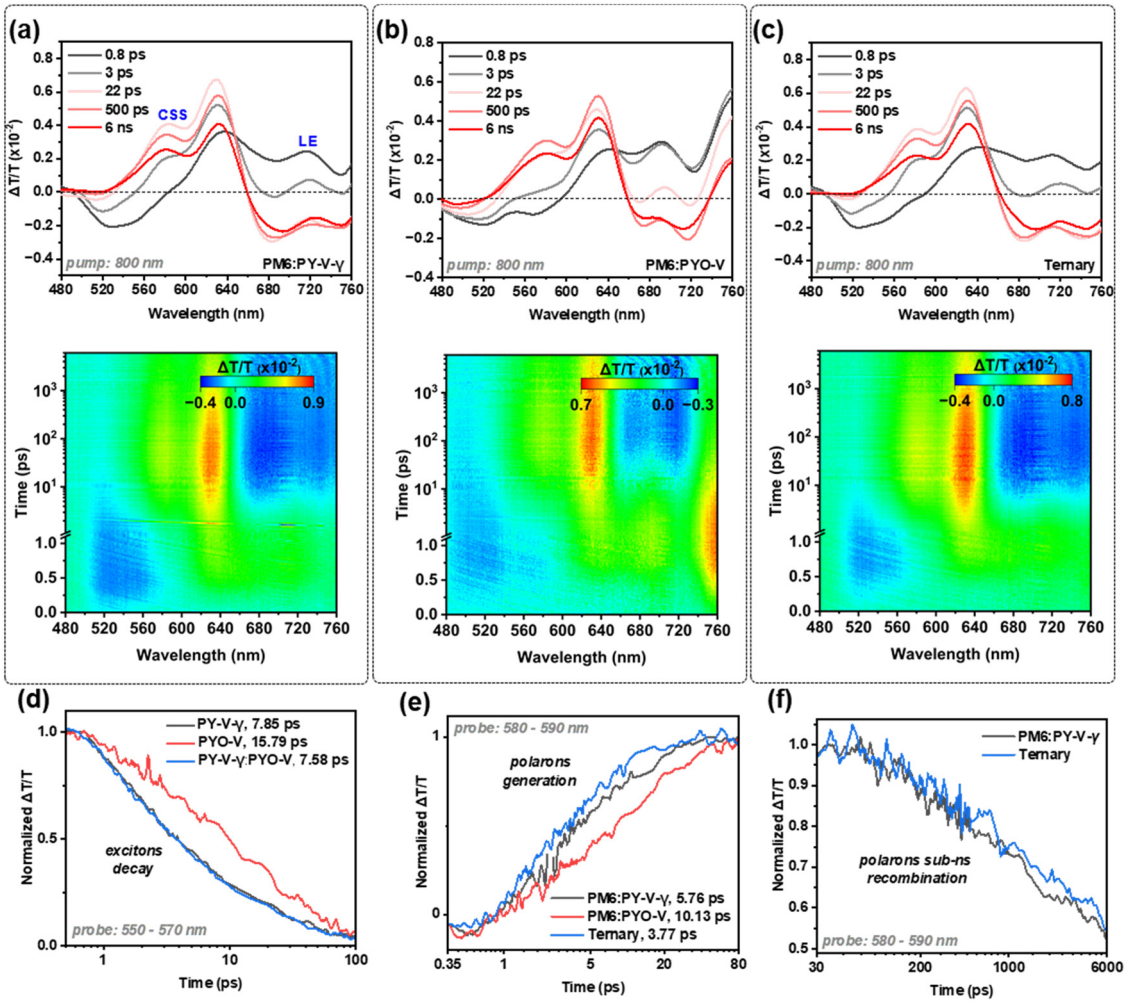

Fig. 4 (a)–(c) Spectral line cuts and pseudo-2D maps of transient absorption for acceptor and donor–acceptor blend thin films at a constant excitation fluence of 2 μJ cm^{-2} with an 800 nm pump wavelength. The corresponding kinetics are also plotted for (d) singlet exciton photo-induced absorption decay, (e) polaron photobleach generation, and (f) polaron recombination at a sub-ns regime.

0.499 eV is among the lowest energy loss values reported for all-PSCs (Fig. 5f), surpassing even those observed in high-performance SMA-based devices.

The operational stability is a crucial assessment for all-PSCs, and so the maximum power point tracking (MPPT) technique was carried out to examine the binary and ternary devices (Fig. 6a and Fig. S12, ESI†). After 70 h, all binary devices displayed a decay to 80% of the initial PCE and essentially dropped to 60% of the initial PCE at ~170 h. In contrast, the ternary device maintained ~70% of the initial PCE at ~170 h. Furthermore, the decay in the J_{SC} value was relatively obvious, and the current decay of the ternary devices was relatively slow. It is evident that the introduction of PYO-V into the PM6:PY-V-γ system can significantly enhance the photothermal stability of the devices. Lastly, the indoor photovoltaic performance of PYO-V was investigated by screening different LED light sources (2600 K, 3000 K, 4000 K and 6500 K) and 2600 K was shown to be the best condition among all the light sources (Fig. 6b), because its emission spectrum matches the most with that of PYO-V. The input power measurement and indoor PCE calculations were performed following the procedure in our previous work. The device performance under the different illumination conditions (2000, 1600, 1000, and 500 lux) of the 2600 K LED lamp was studied in depth (Fig. 6c and d), and the results are summarized in Table 2. It is worth noting that PM6:PYO-V exhibited a PCE of 24.0% at a luminous intensity of 2000 lux, which is the highest performance for indoor all-PSCs to date.

Finally, to evaluate the universality of the PYO-V guest component, we chose another state-of-the-art all-polymer system of PM6:PYF-T-*o* as the host,[47,48] following the same procedure in device fabrication. It was found that ternary devices showed enhanced FFs and PCEs, and the PM6:PYF-T-*o*:PYO-V-based devices achieved the highest efficiency of 16.7% (Fig. S14 and Table S5, ESI†). These results demonstrate the universality of the alkoxy polymer acceptor as the guest component in increasing PCEs of all-PSCs.

Conclusion

In conclusion, a high-performance polymer acceptor PYO-V is constructed successfully by incorporating alkoxy side chains at

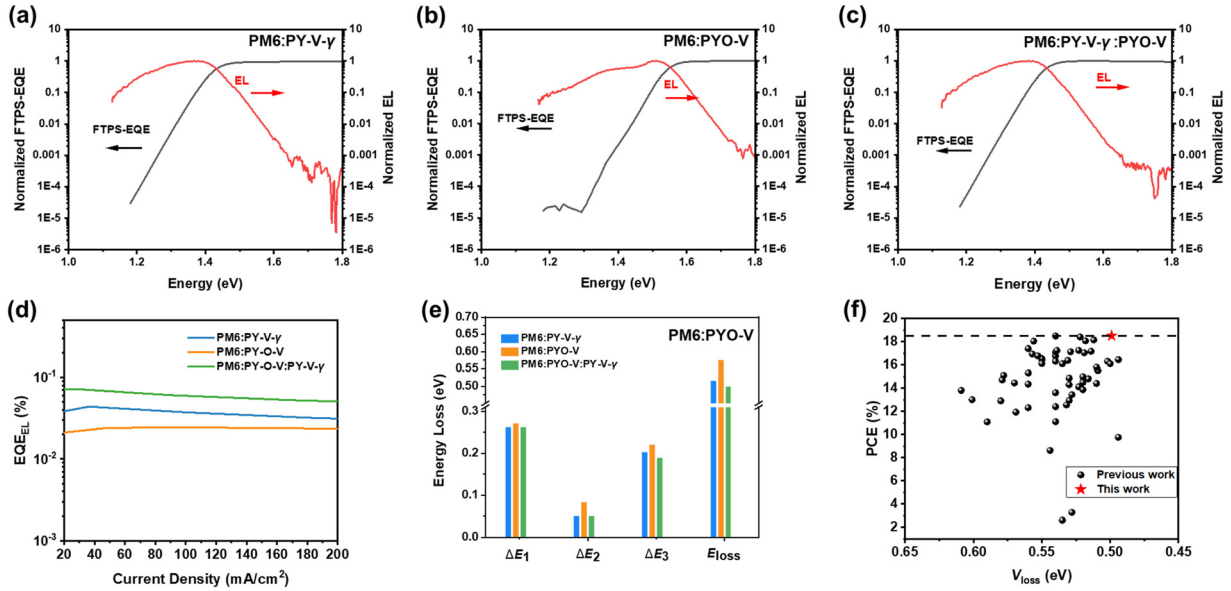

Fig. 5 (a)–(c) Semilogarithmic plots of normalized EL, measured EQE, and EQE calculated using FTPS (EQE-FTPS) as a function of energy for devices. (d) EQE_{EL} spectra. (e) Detailed E_{loss} of devices. (f) All polymer V_{loss} *vs.* PCE.

the β position of the outer thiophene units into Y-series polymer acceptors. The alkoxy side chain functionalization induces a blue shift in the UV-Vis absorption and an upshift in the energy levels. This alteration enables complementary absorption and effective management of energy loss in the host binary system. The resultant PM6:PY-V-γ:PYO-V ternary all-PSCs achieved a significantly improved efficiency of 18.5% with a high V_{OC} of 0.932 V, which is much higher compared to 17.3% for PM6:PY-V-γ-based solar cells. The improved device performance obtained in the ternary device benefits from the synergistic effects of the complementary light-harvesting spectrum, enhanced polaron generation rate, suppressed charge recombination, and decreased energy loss. Moreover, the hypsochromic PYO-V demonstrates its potential in indoor photovoltaics, achieving an efficiency of 24.0% in binary devices. These results highlight the effectiveness of alkoxy substitution as a viable strategy for fine-tuning the optoelectrical properties of polymer acceptors, leading to efficient all-PSCs for versatile photovoltaic applications.

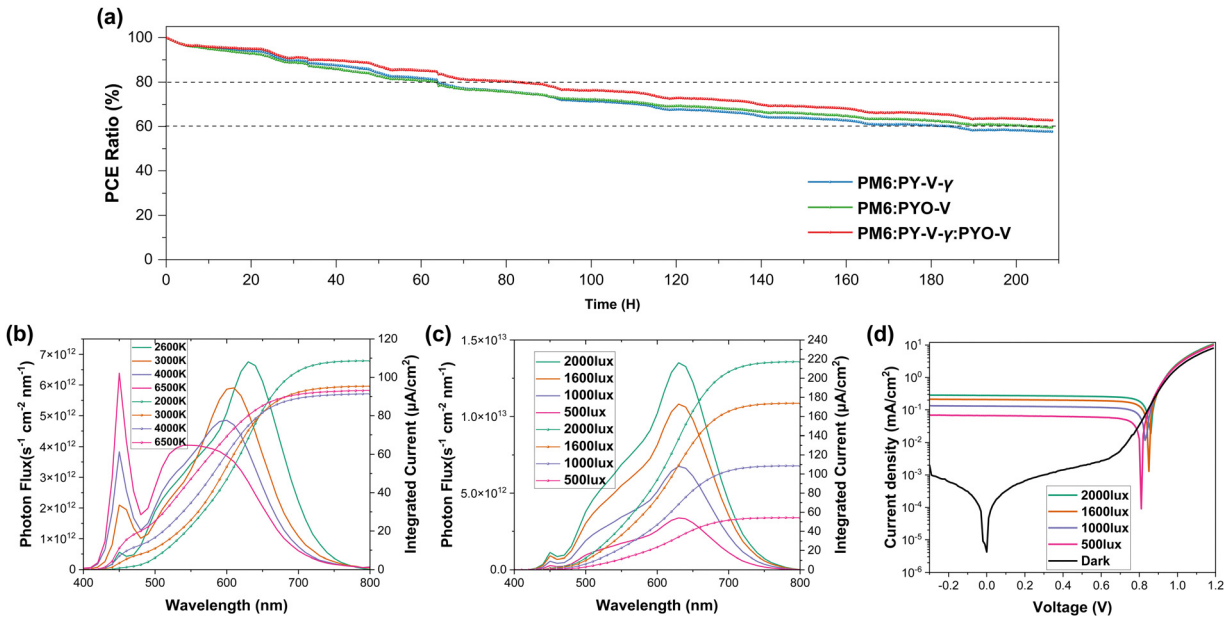

Fig. 6 (a) MPP tracking results for devices of PCE. (b) The photon flux spectrum of 2600, 3000, 4000, and 6500 K LED lamps and the integral current density of PM6:PYO-V under 1000 lux. (c) The photon flux spectrum of a 2600 K LED lamp and the integral current density of PM6:PYOV under 2000, 1600, 1000, and 500 lux. (d) The current density (log scale) as a function of the voltage for PM6:PYO-V under different light conditions.

Table 2 The photovoltaic parameters of PM6:PYO-V under 2600 K LED illumination

Light intensity (lux)	P_{in} (mV cm^{-2})	V_{OC} (V)	J_{SC} (μA cm^{-2})	J_{cal} (μA cm^{-2})	FF (%)	PCE (%)
2000	0.585	0.857 (0.856 ± 0.003)	226.1 (224.1 ± 2.0)	217.2	72.6	24.0
1600	0.468	0.850 (0.849 ± 0.003)	178.5 (177.5 ± 1.0)	173.8	72.3	23.4
1000	0.290	0.834 (0.832 ± 0.004)	111.0 (110.2 ± 0.8)	108.6	71.9	23.0
500	0.145	0.810 (0.808 ± 0.004)	56.4 (55.9 ± 0.5)	54.3	70.3	22.2

Author contributions

H. Yu, C. Z., and H. H. conceived the idea. H. Yu carried out the material synthesis and characterization. C. Z. carried out the device fabrication and measurements. S. Z. performed the GIWAXS measurements. B. Z. performed the TR-PL, TPC and TPV measurements. T. P., M. L. and J. W. helped in TAS measurements. H. N. and C. K. helped in the AFM measurements. J. Y. and W. L. helped in the material characterization studies. H. Yu, C. Z., and H. H. prepared the manuscript. H. Yu, H. H., G. Z. and H. Yan directed and supervised the project. All the authors discussed and commented on the manuscript.

Conflicts of interest

There are no conflicts to declare.

Acknowledgements

This work was supported by the National Natural Science Foundation of China (NSFC, nos. 52103202, 22075057, and 52333006), the National Key Research and Development Program of China (no. 2019YFA0705900) funded by MOST, the Basic and Applied Research Major Program of Guangdong Province (no. 2019B030302007), the Shen Zhen Technology and Innovation Commission (JCYJ20200109140801751), the Hong Kong Research Grants Council (research fellow scheme RFS2021-6S05, RIF project R6021-18, CRF project C6023-19G, and GRF project 16310019, 16310020, 16309221, and 16309822), the Hong Kong Innovation and Technology Commission (ITC-CNERC14SC01), Foshan-HKUST (project no. FSUST19-CAT0202), the Zhongshan Municipal Bureau of Science and Technology (no. ZSST20SC02), the Guangdong-Hong Kong-Macao Joint Laboratory (No. 2023B1212120003) and the Tencent Xplorer Prize. We also would like to express our gratitude to beamline BL16B1 at Shanghai Synchrotron Radiation Facility (SSRF) for their support during the GIWAXS experiment. RSoXS measurement was conducted at ALS BL 11.0.1.2, supported by the Office of Science, Office of Basic Energy Sciences, of the U.S. Department of Energy under contract no. DE-AC02-05CH11231.

References

1 Y. H. Liu, B. W. Li, C. Q. Ma, F. Huang, G. T. Feng, H. Z. Chen, J. H. Hou, L. P. Yan, Q. Y. Wei, Q. Luo, Q. Y. Bao, W. Ma, W. Liu, W. W. Li, X. J. Wan, X. T. Hu, Y. C. Han, Y. W. Li, Y. H. Zhou, Y. P. Zou, Y. W. Chen, Y. F. Li, Y. S. Chen, Z. Tang, Z. C. Hu, Z. G. Zhang and Z. S. Bo, *Sci. China: Chem.*, 2022, **65**, 224–268.
2 G. Zhang, J. Zhao, P. C. Y. Chow, K. Jiang, J. Zhang, Z. Zhu, J. Zhang, F. Huang and H. Yan, *Chem. Rev.*, 2018, **118**, 3447–3507.
3 R. Søndergaard, M. Hösel, D. Angmo, T. T. Larsen-Olsen and F. C. Krebs, *Mater. Today*, 2012, **15**, 36–49.
4 S. Liu, H. Li, X. Wu, D. Chen, L. Zhang, X. Meng, L. Tan, X. Hu and Y. Chen, *Adv. Mater.*, 2022, **34**, 2201604.
5 J. Yi, G. Zhang, H. Yu and H. Yan, *Nat. Rev. Mater.*, 2023, **9**, 46–62.
6 A. Wadsworth, M. Moser, A. Marks, M. S. Little, N. Gasparini, C. J. Brabec, D. Baran and I. McCulloch, *Chem. Soc. Rev.*, 2018, **48**, 1596.
7 L. Lu, T. Zheng, Q. Wu, A. M. Schneider, D. Zhao and L. Yu, *Chem. Rev.*, 2015, **115**, 12666–12731.
8 Q. Wei, J. Yuan, Y. Yi, C. Zhang and Y. Zou, *Nat. Sci. Rev.*, 2021, **8**, nwab121.
9 W. Gao, F. Qi, Z. Peng, F. R. Lin, K. Jiang, C. Zhong, W. Kaminsky, Z. Guan, C.-S. Lee, T. J. Marks, H. Ade and A. K.-Y. Jen, *Adv. Mater.*, 2022, **34**, 2202089.
10 L. Zhu, M. Zhang, J. Xu, C. Li, J. Yan, G. Zhou, W. Zhong, T. Hao, J. Song, X. Xue, Z. Zhou, R. Zeng, H. Zhu, C. C. Chen, R. C. I. MacKenzie, Y. Zou, J. Nelson, Y. Zhang, Y. Sun and F. Liu, *Nat. Mater.*, 2022, **21**, 656–663.
11 K. Chong, X. Xu, H. Meng, J. Xue, L. Yu, W. Ma and Q. Peng, *Adv. Mater.*, 2022, **34**, 2109516.
12 H. Hu, S. Liu, J. Xu, R. Ma, Z. Peng, T. A. D. Peña, Y. Cui, W. Liang, X. Zhou, S. Luo, H. Yu, M. Li, J. Wu, S. Chen, G. Li and Y. Chen, *Angew. Chem., Int. Ed.*, 2024, **63**, e202400086.
13 M. Kataria, H. D. Chau, N. Y. Kwon, S. H. Park, M. J. Cho and D. H. Choi, *ACS Energy Lett.*, 2022, **7**, 3835–3854.
14 Z. G. Zhang and Y. Li, *Angew. Chem., Int. Ed.*, 2021, **60**, 4422–4433.
15 P. Cheng and X. Zhan, *Chem. Soc. Rev.*, 2016, **45**, 2544–2582.
16 J. Yuan, Y. Q. Zhang, L. Y. Zhou, G. C. Zhang, H. L. Yip, T. K. Lau, X. H. Lu, C. Zhu, H. J. Peng, P. A. Johnson, M. Leclerc, Y. Cao, J. Ulanski, Y. F. Li and Y. P. Zou, *Joule*, 2019, **3**, 1140–1151.
17 K. Jiang, Q. Wei, J. Y. L. Lai, Z. Peng, H. K. Kim, J. Yuan, L. Ye, H. Ade, Y. Zou and H. Yan, *Joule*, 2019, **3**, 3020–3033.
18 J. Ge, L. Xie, R. Peng and Z. Ge, *Adv. Mater.*, 2022, **34**, 2206566.
19 P. Murugan, T. Hu, X. Hu and Y. Chen, *J. Mater. Chem. A*, 2022, **10**, 17968–17987.
20 W. Wang, Q. Wu, R. Sun, J. Guo, Y. Wu, M. Shi, W. Yang, H. Li and J. Min, *Joule*, 2020, **4**, 1070–1086.
21 H. Yu, Z. Qi, J. Yu, Y. Xiao, R. Sun, Z. Luo, A. M. H. Cheung, J. Zhang, H. Sun, W. Zhou, S. Chen, X. Guo, X. Lu, F. Gao, J. Min and H. Yan, *Adv. Energy Mater.*, 2020, **11**, 2003171.

22 J. Jia, Q. Huang, T. Jia, K. Zhang, J. Zhang, J. Miao, F. Huang and C. Yang, *Adv. Energy Mater.*, 2021, **12**, 2103193.
23 H. K. Kim, H. Yu, M. Pan, X. Shi, H. Zhao, Z. Qi, W. Liu, W. Ma, H. Yan and S. Chen, *Adv. Sci.*, 2022, **9**, 2202223.
24 H. Yu, Y. Wang, X. Zou, J. Yin, X. Shi, Y. Li, H. Zhao, L. Wang, H. M. Ng, B. Zou, X. Lu, K. S. Wong, W. Ma, Z. Zhu, H. Yan and S. Chen, *Nat. Commun.*, 2023, **14**, 2323.
25 H. Yu, Y. Wang, H. K. Kim, X. Wu, Y. Li, Z. Yao, M. Pan, X. Zou, J. Zhang, S. Chen, D. Zhao, F. Huang, X. Lu, Z. Zhu and H. Yan, *Adv. Mater.*, 2022, **34**, 2200361.
26 C. Zhao, R. Ma, Y. Hou, L. Zhu, X. Zou, W. Xiong, H. Hu, L. Wang, H. Yu, Y. Wang, G. Zhang, J. Yi, L. Chen, D. Wu, T. Yang, G. Li, M. Qiu, H. Yan, S. Li and G. Zhang, *Adv. Energy Mater.*, 2023, **13**, 2300904.
27 Y. Yue, B. Zheng, J. Ni, W. Yang, L. Huo, J. Wang and L. Jiang, *Adv. Sci.*, 2022, **9**, 2204030.
28 X. Yang, R. Sun, Y. Wang, M. Chen, X. Xia, X. Lu, G. Lu and J. Min, *Adv. Mater.*, 2022, **35**, 2209350.
29 C. Y. Zhao, J. C. Yi, L. H. Wang, G. Y. Lu, H. Huang, H. Kim, H. Yu, C. Xie, P. You, G. H. Lu, M. X. Qiu, H. Yan, S. P. Li and G. Y. Zhang, *Nano Energy*, 2022, **104**, 107872.
30 Y. Cai, C. Xie, Q. Li, C. Liu, J. Gao, M. H. Jee, J. Qiao, Y. Li, J. Song, X. Hao, H. Y. Woo, Z. Tang, Y. Zhou, C. Zhang, H. Huang and Y. Sun, *Adv. Mater.*, 2023, **35**, 2208165.
31 H. Yu, S. Luo, R. Sun, I. Angunawela, Z. Qi, Z. Peng, W. Zhou, H. Han, R. Wei, M. Pan, A. M. H. Cheung, D. Zhao, J. Zhang, H. Ade, J. Min and H. Yan, *Adv. Funct. Mater.*, 2021, **31**, 2100791.
32 Y. Cai, C. Xie, Q. Li, C. Liu, J. Gao, M. H. Jee, J. Qiao, Y. Li, J. Song, X. Hao, H. Y. Woo, Z. Tang, Y. Zhou, C. Zhang, H. Huang and Y. Sun, *Adv. Mater.*, 2022, **34**, 2208165.
33 Y. Chen, H. Meng, L. Ding, J. Tang, J. Yi, J. Zhang, Z. Wang, R. Ma, Z. Li, L. Lyu, X. Xu, R. Li, Q. Peng, H. Yan and H. Hu, *Chem. Mater.*, 2022, **34**, 10144–10152.
34 Y. Chen, F. Bai, Z. Peng, L. Zhu, J. Zhang, X. Zou, Y. Qin, H. K. Kim, J. Yuan, L. K. Ma, J. Zhang, H. Yu, P. C. Y. Chow, F. Huang, Y. Zou, H. Ade, F. Liu and H. Yan, *Adv. Energy Mater.*, 2020, **11**, 2003141.
35 J. Liang, M. Pan, Z. Wang, J. Zhang, F. Bai, R. Ma, L. Ding, Y. Chen, X. Li, H. Ade and H. Yan, *Chem. Mater.*, 2022, **34**, 2059–2068.
36 Y. Cui, Y. Wang, J. Bergqvist, H. Yao, Y. Xu, B. Gao, C. Yang, S. Zhang, O. Inganäs, F. Gao and J. Hou, *Nat. Energy*, 2019, **4**, 768–775.
37 Y. Cai, Q. Li, G. Lu, H. S. Ryu, Y. Li, H. Jin, Z. Chen, Z. Tang, G. Lu, X. Hao, H. Y. Woo, C. Zhang and Y. Sun, *Nat. Commun.*, 2022, **13**, 2369.
38 C. M. Proctor, S. Albrecht, M. Kuik, D. Neher and T.-Q. Nguyen, *Adv. Energy Mater.*, 2014, **4**, 1400230.
39 G. G. Malliaras, J. R. Salem, P. J. Brock and C. Scott, *Phys. Rev. B: Condens. Matter Mater. Phys.*, 1998, **58**, R13411.
40 Y. Zeng, D. Li, Z. Xiao, H. Wu, Z. Chen, T. Hao, S. Xiong, Z. Ma, H. Zhu, L. Ding and Q. Bao, *Adv. Energy Mater.*, 2021, **11**, 2101338.
41 T. Xiao, J. Wang, S. Yang, Y. Zhu, D. Li, Z. Wang, S. Feng, L. Bu, X. Zhan and G. Lu, *J. Mater. Chem. A*, 2020, **8**, 401–411.
42 E. Gann, A. T. Young, B. A. Collins, H. Yan, J. Nasiatka, H. A. Padmore, H. Ade, A. Hexemer and C. Wang, *Rev. Sci. Instrum.*, 2012, **83**, 045110.
43 Z. Wang, W. Liang, X. Zhou, S. Zhu, W. Xiong, J. Xu and H. Hu, *ACS Appl. Polym. Mater.*, 2023, **5**, 9329–9336.
44 R. Wang, C. Zhang, Q. Li, Z. Zhang, X. Wang and M. Xiao, *J. Am. Chem. Soc.*, 2020, **142**, 12751–12759.
45 D. Qian, Z. Zheng, H. Yao, W. Tress, T. R. Hopper, S. Chen, S. Li, J. Liu, S. Chen, J. Zhang, X. K. Liu, B. Gao, L. Ouyang, Y. Jin, G. Pozina, I. A. Buyanova, W. M. Chen, O. Inganas, V. Coropceanu, J. L. Bredas, H. Yan, J. Hou, F. Zhang, A. A. Bakulin and F. Gao, *Nat. Mater.*, 2018, **17**, 703–709.
46 M. Azzouzi, T. Kirchartz and J. Nelson, *Trend. Chem.*, 2019, **1**, 49–62.
47 H. Yu, M. Pan, R. Sun, I. Agunawela, J. Zhang, Y. Li, Z. Qi, H. Han, X. Zou, W. Zhou, S. Chen, J. Y. L. Lai, S. Luo, Z. Luo, D. Zhao, X. Lu, H. Ade, F. Huang, J. Min and H. Yan, *Angew. Chem., Int. Ed.*, 2021, **60**, 10137–10146.
48 H. Yu, Y. Wang, X. Zou, H. Han, H. K. Kim, Z. Yao, Z. Wang, Y. Li, H. M. Ng, W. Zhou, J. Zhang, S. Chen, X. Lu, K. S. Wong, Z. Zhu, H. Yan and H. Hu, *Adv. Funct. Mater.*, 2023, **33**, 2300712.